Chemical Engineering Journal 165 (2010) 250–257

Contents lists available at ScienceDirect

Chemical Engineering Journal

journal homepage: www.elsevier.com/locate/cej

UV-light induced photocatalytic decolorization of Rhodamine 6G molecules over BiOCl from aqueous solution

M.A. Gondal[a,b,*], X.F. Chang[b,c], Z.H. Yamani[a,b]

[a] Laser Research Group, Physics Department, King Fahd University of Petroleum and Minerals, Dhahran 31261, Saudi Arabia
[b] Center of Excellence in Nanotechnology, King Fahd University of Petroleum and Minerals, KFUPM Box 741, Dhahran 31261, Saudi Arabia
[c] Department of Applied Chemistry, College of Materials Science and Technology, Nanjing University of Aeronautics and Astronautics, Nanjing 211100, China

ARTICLE INFO

Article history:
Received 30 July 2010
Received in revised form
19 September 2010
Accepted 20 September 2010

Keywords:
BiOCl
Sorption kinetics
Sorption isotherm
Photocatalytic
Rhodamine 6G
Pulsed-laser
Mulliken electronegativity

ABSTRACT

The sorption and photocatalytic decolorization (under irradiation of monochromaticitic 355 nm-pulsed-laser) behaviors of Rhodamine 6G (Rh 6G) in presence of BiOCl semiconductor in aqueous solution were studied in this paper. The sorption kinetic and isotherm behaviors of Rh 6G over BiOCl catalyst were investigated and discussed through pseudo-second-order/intraparticle diffusion models and Langmuir/Freundlich models, respectively. The effect of critical parameters such as catalyst dosage, initial concentration of Rh 6G, and laser pulse energy on the photocatalytic decolorization process was investigated. The photocatalytic decolorization and photonic efficiency of BiOCl was compared with standard catalyst (TiO_2) and the obtained results were discussed in terms of their band edge position. Finally, the chemical stability of BiOCl photocatalyst was studied by measuring the X-ray diffraction (XRD) pattern of BiOCl samples after the reaction.

1. Introduction

During the last few decades, considerable attention has been directed towards the use of semiconductors (as represented by TiO_2) to oxidize organic contaminants and such method is considered to be one of the most promising industrial effluent water treatment processes [1]. Recently, bismuth oxyhalides, BiOX (X = Cl, Br, I), have received much interests due to their potential applications in decomposing organic compounds for environmental remediation [2–11], photo-electrochemical conversion [12] and splitting water into hydrogen and oxygen gases [6].

Bismuth oxychloride (BiOCl) is a wide bandgap semiconductor with a band gap value of 3.19–3.44 eV [2,5,6,10,13]. In recent studies, it has been reported that BiOCl can be effectively used as photocatalyst to decompose organic pollutants under UV and UV–vis light irradiation [2,5]. Moreover, the photocatalytic response of BiOCl was found to be better than that of commercial Degussa P25 (TiO_2), in spite of their similar band gap values. These initial results demonstrated that BiOCl could be used as a potential photocatalyst under UV light irradiation and can compete with TiO_2.

Recently, owing to the unique properties like monochromaticity, high intensity, and low beam divergence, lasers have been used in our laboratory and elsewhere to achieve high efficiencies in photocatalytic splitting of water [14,15], decomposition of toxic organic matters [16,17], and antimicrobial applications [18]. In the present study, the sorption and pulsed-laser-induced (λ = 355 nm) photocatalytic decolorization behaviors of Rhodamine 6G (Rh 6G) in presence of BiOCl semiconductor in aqueous solution were studied systematically. The initial photocatalytic decolorization efficiencies of BiOCl and P25 were compared and discussed based on the band edge position calculation results. In addition, the crystal-structure stability of BiOCl photocatalyst during laser-induced photocatalysis and the possible catalytic process was initially investigated and discussed as well.

2. Experimental

2.1. Materials and reagents

TiO_2 (product name P25; Mw: 79.9 g/mol; 80% anatase and 20% rutile; BET specific surface area: 50 m^2/g, agglomerated P25 parti-

* Corresponding author at: Laser Research Group, Physics Department, King Fahd University of Petroleum and Minerals, Box 372, Dhahran 31261, Saudi Arabia. Tel.: +966 38602351; fax: +966 38602293.
E-mail address: magondal@kfupm.edu.sa (M.A. Gondal).

1385-8947/$ – see front matter © 2010 Elsevier B.V. All rights reserved.
doi:10.1016/j.cej.2010.09.025

cle size: 30–50 nm, approximately) was kindly supplied by Degussa Company. BiOCl photocatalyst with sheet morphology (Mw: 260.5 g/mol; BET surface area was determined to be 1.74 m^2/g, the sheet size and thickness was roughly measured at 700 nm and 30 nm, respectively) was prepared according to the previous report [10]. The target pollutant Rh 6G (analytic grade, Mw: 479.02 g/mol) was provided by Merck Company. Distilled water was used for the preparation of solutions and all chemicals were used without further purification.

2.2. Characterization of photocatalyst

The crystal structure of BiOCl was determined by X-ray diffractometer (XRD, Bruker D8 ADVANCE) using Cu-Kα X-ray source (λ = 0.15418 nm). The N_2 adsorption–desorption analysis was carried out on a NOVA 4000 (Quantachrome Corporation) instrument. Diffuse reflectance spectroscopy (UV–vis) DRS measurement was performed at room temperature on a Hitachi U-3010 spectrophotometer by using $BaSO_4$ as reference.

2.3. Adsorption kinetics/isotherm experiment

Adsorption kinetics experiment was carried out with a thermostatic shaker at 150 rpm at 298 K. Experiment was performed by placing 0.1 g of BiOCl sample in a glass flask containing 200 mL of Rh 6G solution at 7 and 15 ppm. 2–4 mL Rh 6G solution was sampled from the glass flask at certain time intervals. Adsorption isotherm experiment was carried out with a thermostatic shaker at 150 rpm at 298 K for 48 h and experiments were performed using a batch equilibrium technique by placing 0.1 g of BiOCl sample in a glass flask containing 200 mL of Rh 6G solution at various concentrations. The change in concentration of Rh 6G was monitored by UV–vis spectrometer (JASCO, V-570) at wavelength of 526 nm.

2.4. Photocatalysis experiment

A 355 nm wavelength high power laser beam, generated from the third harmonic of the Spectra Physics Nd:YAG laser (Model GCR 250) with a pulse width of ~8 ns, was employed as the light source and the diameter of laser beam was expanded to ~1.0 cm to avoid the destructive effect of radiation. The experimental setup used to study the photocatalytic reaction was described in detail in our earlier publication [16]. The photonic efficiency (PE) for the photocatalytic reaction was calculated as well in order to further evaluate the catalytic performance. The calculation method is given as follows:

$$\text{photonic efficiency \%} = \frac{\text{number of dye molecules decomposed/time}}{\text{number of photons of wavelength } \lambda \text{ absorbed/time}} \times 100\% \quad (1.1)$$

$$\text{number of photons of wavelength } \lambda \text{ absorbed} = \frac{E_L \cdot t}{h\nu} \quad (1.2)$$

where E_L is the laser energy in Joule, t the time in seconds, h the Planks constant and ν is the frequency of the incident laser. Thus the photonic efficiency (%) can be described through the expression of total number of dyes molecules decomposed divided by total number of photons of laser incident and multiply by 100. In addition, a 6 W UV germicidal lamp was employed as a UV light source for comparison with laser. During all the photocatalytic reactions, the volume of the solution was controlled at 150 mL.

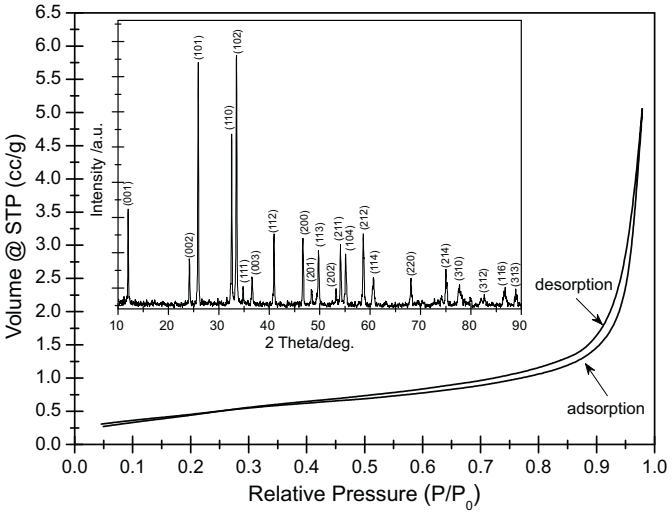

Fig. 1. N_2 adsorption–desorption isotherm and XRD pattern (inset) of BiOCl photocatalyst.

3. Results and discussion

3.1. Microstructure characterization

In the X-ray diffraction pattern shown in Fig. 1 (inset), all the diffraction peaks match well with the crystal structure of the tetragonal BiOCl phase (space group: P4/nmm (129), JCPDS No. 82-0485). The presented hysteresis loop in N_2 adsorption–desorption curves (as given in Fig. 1) shows the small amount of pore structures in BiOCl photocatalyst owning to the stacking of the sheet-like morphology of BiOCl [10]. The result of N_2 adsorption–desorption suggested the BET specific surface area of BiOCl was 1.74 m^2/g. The band gap of BiOCl photocatalyst was calculated at 3.2–3.5 eV through UV–vis DRS measurement and Tuac's approach (as shown in Fig. 2) [19,20]. The characterization results mentioned above demonstrate the high purity, low specific surface area, poor pore-structure and the similar bandgap-value between TiO_2 and as-prepared BiOCl sample.

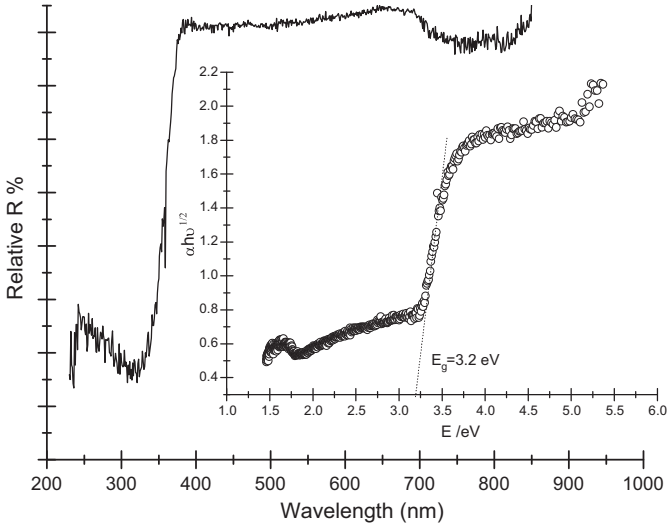

Fig. 2. UV–vis DRS of BiOCl photocatalyst and its relationship between E_{photon} and $(E_{photon})^{1/2}$ by Tauc approach.

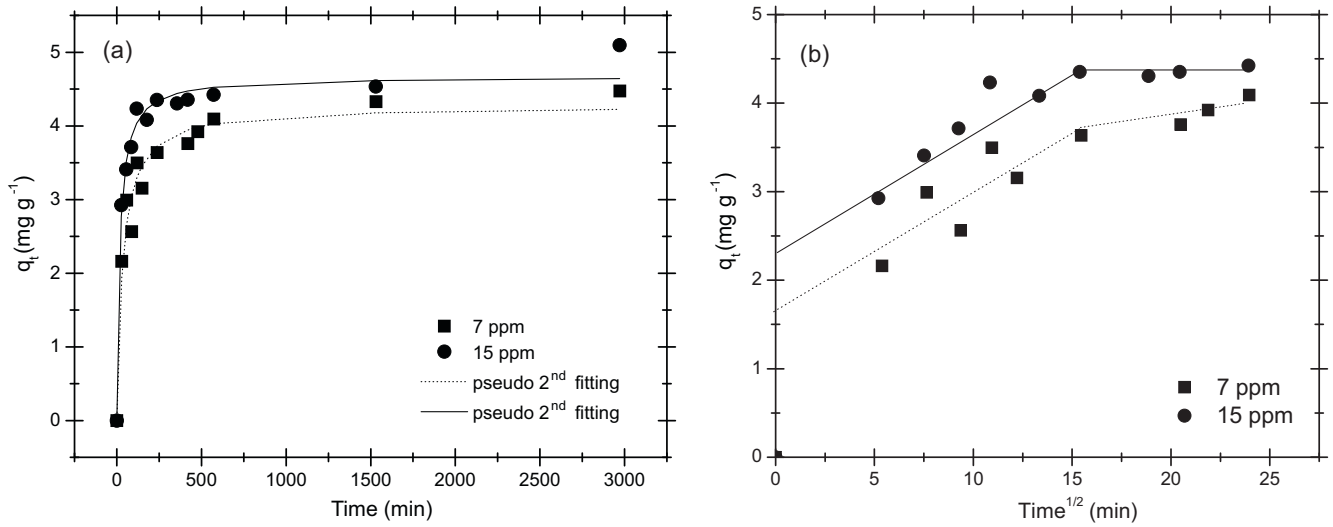

Fig. 3. (a) The adsorption capacity variations of Rh 6G with adsorption time on BiOCl and (b) their intraparticle diffusion models (experimental condition: T = 298 K; initial concentration of Rh 6G = 7 and 15 ppm; BiOCl dosage = 0.5 g/L).

3.2. Sorption kinetics and isotherm

The sorption behavior of Rh 6G molecules on the surface of BiOCl catalyst is a significant process during photocatalysis. As shown in Fig. 3(a), the dependence of Rh 6G adsorption capacity on contact time between Rh 6G and BiOCl catalyst, suggests that the adsorption–desorption equilibrium can be obtained after contact time of 25 h. The pseudo-second-order model which assumes that the sorption rate is controlled by chemical sorption and the sorption capacity is proportional to the number of active sites on the adsorbent [21] was used to fit the kinetic data, in order to obtain the adsorption kinetics of Rh 6G molecules on BiOCl. The pseudo-second-order model can be expressed in the form as follows:

$$\frac{t}{q_t} = \frac{1}{kq_{eq}^2} + \frac{1}{q_{eq}}t \tag{1.3}$$

where t is the adsorption time, q_t the adsorption capacity for a specific time, k (g/mg min) the rate constant of pseudo-second-order adsorption and q_{eq} (mg/g) the equilibrium adsorption capacity. Table 1 and Fig. 3(a) give the fitted results of pseudo-second-order model, demonstrating the good correlation coefficients ($r^2 > 0.96$) for the pseudo-second-order kinetic model by using BiOCl catalyst, implying the interaction of chemical adsorption could possibly occurred during the sorption process.

The external diffusion and intraparticle diffusion are generally considered as two important steps during a typical sorption process [22]. In order to investigate the rate-control step in our adsorption of Rh 6G molecules on BiOCl catalyst, the intraparticle diffusion model (which can be expressed as follows) was adopted:

$$q_t = k_p t^{1/2} + C \tag{1.4}$$

where k_p (mg/(g h$^{0.5}$)) is the intraparticle diffusion rate constant and C is the intercept. The relevant fitting results given in Table 1 and Fig. 3(b) clearly shows that the adsorption process have relative well fitting linear relationship between q_t and $t^{-0.5}$ lasting for 240 min, but not passing through the origin point, implying that contribution of intraparticle diffusion is not the rate-controlling step [23]. Thus it can be concluded that external diffusion, or both of external and intraparticle diffusions are the rate-controlling step [22]. This is because Rh 6G molecules could possibly diffuse into the inner pore-structures of BiOCl catalyst (as displayed in Fig. 1).

The Langmuir and Freundlich isotherm models were selected to evaluate the adsorption capacity of adsorbents and understand the interactions between adsorbate and adsorbent, which assumes that the sorption occurred at the specific homogeneous sites within the adsorbent and as the adsorbate concentration in solution increases so too does the concentration of adsorbate on the adsorbent surface [24,25]. These two models can be expressed respectively as:

$$q_e = \frac{bq_m C_e}{1 + bC_e} \tag{1.5}$$

$$q_e = KC_e^{1/n} \tag{1.6}$$

where q_e is the equilibrium concentration (mg/L), q_e the amount of Rh 6G adsorbed (mg/g), q_m the theoretical monolayer capacity (mg/g) and b is the adsorption equilibrium constant (L/mg). K (mg$^{1-1/n}$ L$^{1/n}$/g) and n are the Freundlich constants representing the adsorption capacity and adsorption intensity, respectively.

As given in Table 2 and Fig. 4, the sorption isotherm of Rh 6G molecules on BiOCl can be fitted well by both Langmuir and Freundlich model. The theoretical monolayer capacity q_m of BiOCl was calculated at 6.26626 mg/g by Langmuir fitting as well. It is worth noting that although Langmuir equation is derived from the assumption of monolayer coverage, it is not reasonable to deduce

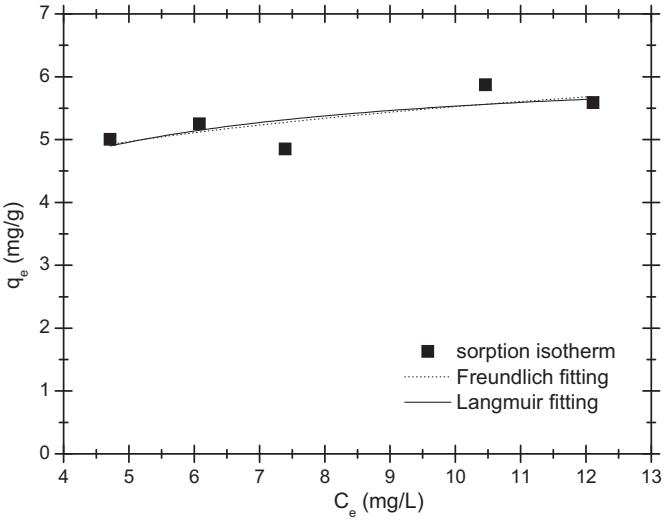

Fig. 4. Adsorption isotherms of Rh 6G on the BiOCl and modeling using the Langmuir and Freundlich equations (experimental condition: T = 298 K; BiOCl dosage = 0.5 g/L).

Table 1
Kinetic parameters of the pseudo-second-order and intraparticle–diffusion models for Rh 6G adsorption on BiOCl at 298 K.

Initial Rh 6G concentration (mg/L)	Pseudo second order kinetic model			Intra-particle diffusion model		
	q_e (mg/g)	k	r^2	k_p (mg/g min$^{1/2}$).	C (mg/g)	r^2
7	4.27305	0.00688	0.98074	0.13491	1.62921	0.69205
15	4.67122	0.01153	0.96028	0.13574	2.3942	0.85743

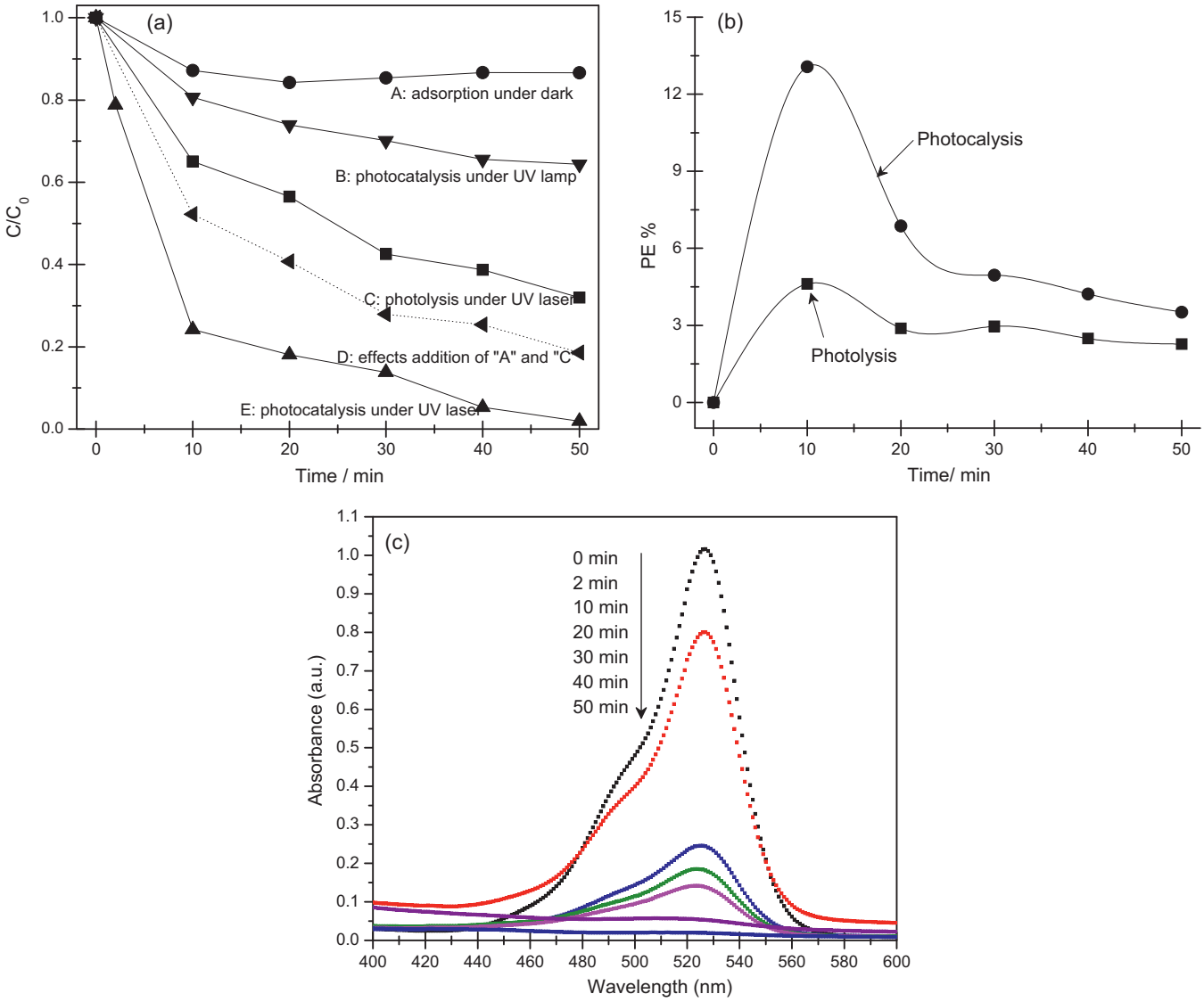

Fig. 5. Rh 6G was only photolyzed, adsorbed in the dark, and photocatalytically decolorized over BiOCl (a), the plots of photonic efficiency versus laser exposure time for BiOCl semiconductor catalysts and photolysis (b), and visible light spectral changes of Rh 6G in BiOCl dispersions as a function of irradiation time (c). Contribution to the sum of photolysis and adsorption was also calculated and shown in (a). Experimental conditions: dosage = 0.4 g/L, initial concentration C_0 = 7 ppm, laser plus energy = 58.6–60.2 mJ.

that the monolayer coverage adsorption process of Rh 6G molecules on the adsorbents could be occurred, and the plateau regions in the sorption isotherms of Rh 6G on such BiOCl could possibly be the result of the condensed liquid being filled in pores of the catalyst [26].

3.3. Effect of irradiation time

The effect of irradiation time on the photocatalytic decolorization of Rh 6G in the presence of BiOCl was investigated and obtained result is depicted in Fig. 5(a). Rh 6G which was only photolyzed and

Table 2
Parameters of Langmuir and Freundlich adsorption models for Rh 6G molecules on BiOCl at 298 K.

Freundlich model			Langmuir model		
K(mg$^{1-1/n}$ L$^{1/n}$/g)	$1/n$	r^2	q_m (mg/g)	b (L/mg)	r^2
3.88563	0.15282	0.71192	6.26626	0.76462	0.75136

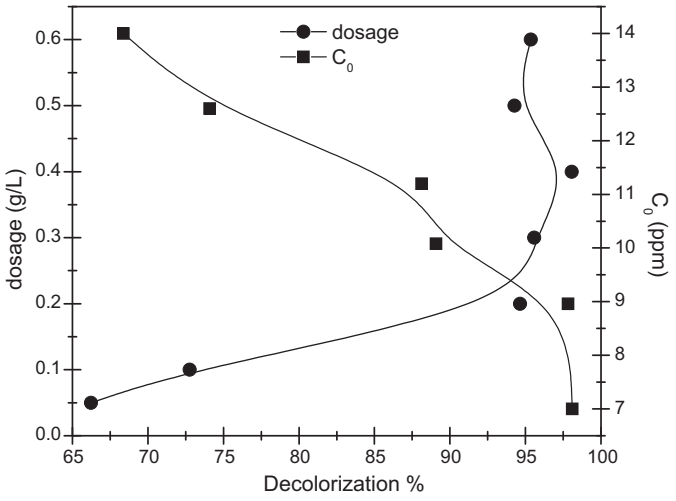

Fig. 6. Effects of dosage and initial concentration on the photocatalytic performance over BiOCl. Experimental conditions: reaction time = 20 min, laser plus energy = 59.1–60.9 mJ, C_0 = 7 ppm (for dosage effect study); reaction time = 20 min, laser plus energy = 60.7–61.3 mJ, dosage = 0.4 g/L (for dosage effect study).

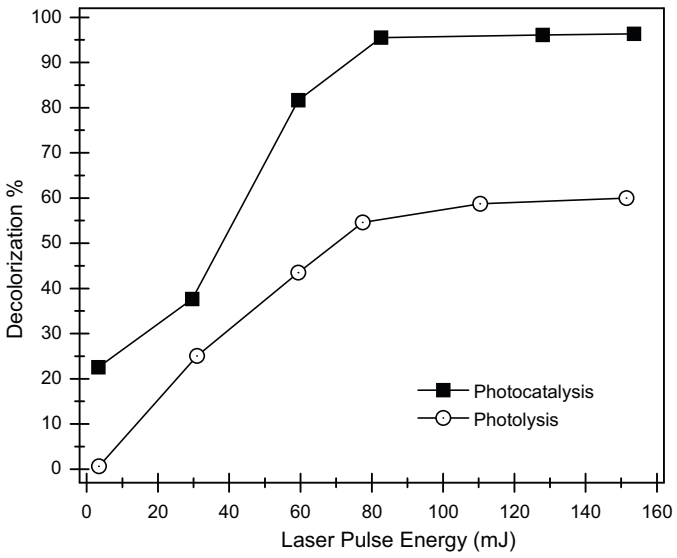

Fig. 7. Dependence of dye decolorization % on the incident laser energy through photocatalysis and photolysis. Experimental conditions: dosage = 0.4 g/L, initial concentration C_0 = 7 ppm, reaction time = 20 min.

adsorbed in the dark was also studied as a comparison. The results indicated that approximately 68% of Rh 6G was decomposed photolytically (the highest PE value was 4.6% at 10 min, as shown in Fig. 5b) and around 13% was adsorbed on the surface of photocatalyst after 50 min reaction. When BiOCl was used as photocatalyst, it catalyzed the photolytic decolorization of Rh 6G effectively and the photocatalytic decolorization of dye was reached to 98% (the highest PE value was calculated at 13.1% after photocatalysis for 10 min, as shown in Fig. 5b) after 50 min under identical conditions. The contribution to the sum of photolysis and adsorption was also calculated and shown in Fig. 5(a), proving the synergetic effect of the photocatalysis reaction. From the photocatalytic kinetic curve shown in Fig. 5(a), the decomposition of Rh 6G was found to be very fast at the beginning of several minutes and then it became slower with increasing the reaction time, which is one of the typical characteristics of pseudo first order kinetics. The displayed UV spectral variations (Fig. 5c) during the photocatalysis demonstrated the absorbance intensity decreasing of the major absorption peak at 526 nm which was attributed to the conjugated structure, and the absorption peak was not apparent after 50 min reaction. In addition during the comparison studies using laser and UV lamp, it was noticed that the photocatalytic decolorization efficiency (only about 35.3%) was much lower using conventional UV lamp as the light source as compared to pulsed laser, demonstrating the high efficiency within short time of this new combined method utilizing photocatalyst and pulsed laser.

3.4. Effect of catalyst dosage and initial Rh 6G concentration

The effect of catalyst dosage on the photocatalytic decolorization process of dye was investigated using different amount of BiOCl varying from 0.05 to 0.6 g/L. It was found that the catalyst dosage can also affect the photocatalytic performance dramatically (Fig. 6) and there was an optimum amount of BiOCl catalyst for the maximum decolorization of dye. The decomposition of the target pollutant was found to increase with the increase in catalyst amount up to the value of 0.4 g/L and a further increase in catalyst dosage could not contribute in the enhancement of photocatalytic decolorization process which is in agreement with previous studies [27,28]. It is not difficult to understand that lower catalytic activity was exhibited under low catalyst dosage, because of smaller amount of catalytic active sites. But nevertheless, the decolorization starts to be saturated if the dosage is much higher than the optimal value because an increase in opacity and light scattering of BiOCl and a decrease in the number of catalytic surface active sites caused by aggregation of BiOCl particles under high dosage amount [28].

The influence of initial Rh 6G concentration (varying from 7 to 14 ppm) on the photocatalytic decolorization process is given in Fig. 6. The decolorization rate (%) was estimated to be 98.1%, 97.8%, 89.1%, 88.1%, 74.1% and 68.4% for initial concentrations of Rh 6G of 7.0 ppm, 8.96 ppm, 10.08 ppm 11.2 ppm, 12.6 pm and 14.0 ppm, respectively. The trend of Rh 6G decolorization shows a strong dependence on its initial concentration and the decolorization rate increases with the decreasing initial concentration and such tendency is in agreement with the Langmuir–Hinshelwood rate expression which has been successfully used for describing the heterogeneous photocatalytic kinetic process [29].

3.5. Effect of laser energy

The laser energy is a significant parameter to control the laser-induced photocatalytic reaction. The effect of incident laser pulse energy on the photocatalytic and photolytic decolorization of Rh 6G was studied and the obtained results are presented in Fig. 7. It is obvious from Fig. 7 that the decolorization rate becomes almost independent on the laser energy in both, photocatalysis and photolysis, the processes. This phenomenon may be attributed to the fact that an increase in laser energy can generate higher number of photons and thereby the number of the actives species (such as OH radicals) in the reaction media and consequently the photocatalytic and photolytic decolorization of dye under investigation. When the incident laser pulse energy was kept 3.3 mJ, the photocatalytic decolorization was estimated to be ~22.5% after reaction of 20 min and about 95% Rh 6G decolorization was obtained when the laser energy was increased to 82 mJ. However, in case of photolysis process, only 60% decolorization rate was obtained when the incident laser pulse energy was 151 mJ.

3.6. Photocatalytic activity comparison between BiOCl and P25

The photocatalytic activity of Degussa P25, a standard photocatalyst, was also evaluated under identical experimental conditions

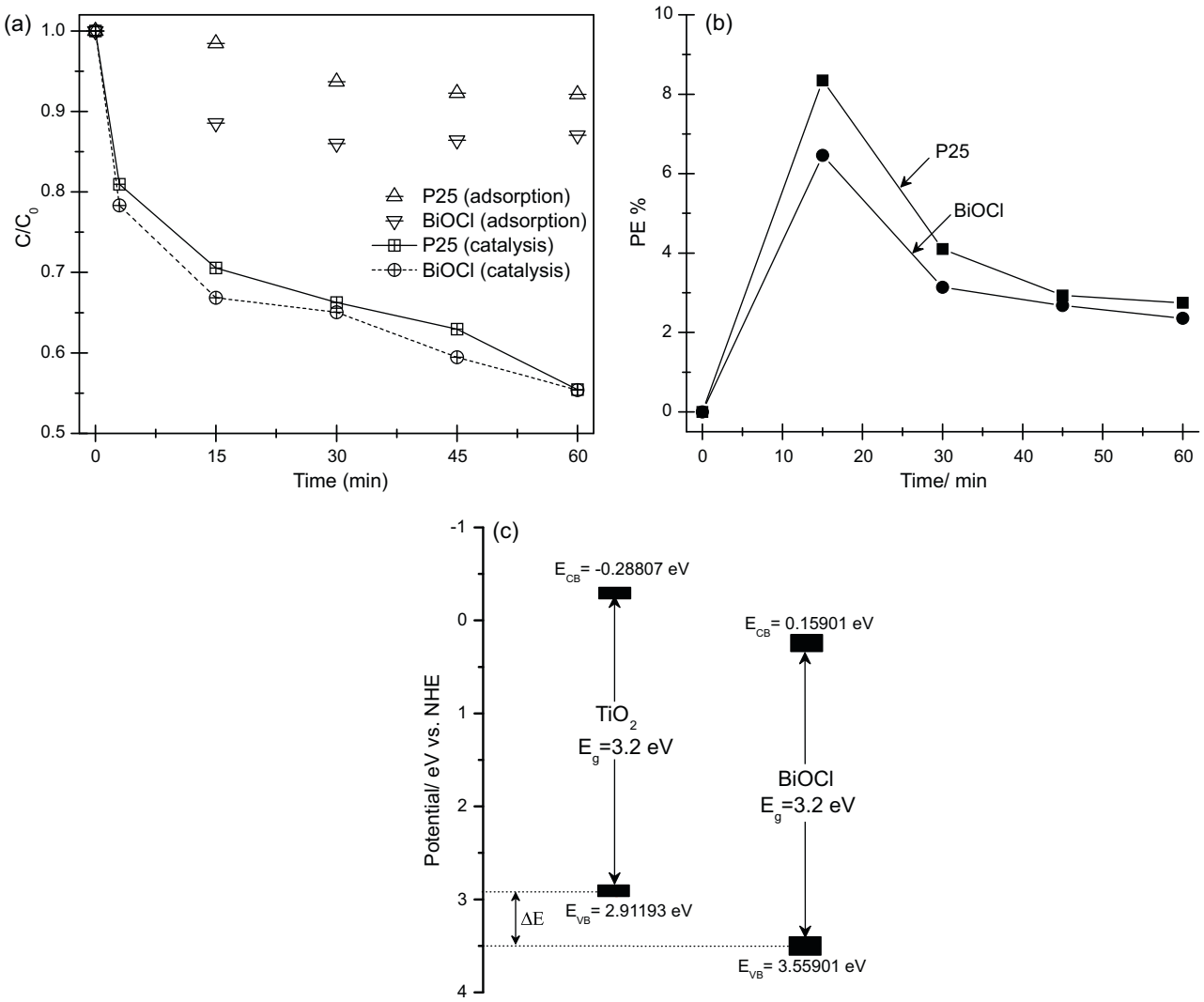

Fig. 8. Photocatalytic activity comparison between BiOCl and P25 (a), plots of photonic efficiency versus laser exposure time for BiOCl and P25 semiconductor catalysts (b) and energetic diagrams of BiOCl and TiO_2 (c). Experimental conditions: dosage = 1 mmol/150 mL; initial concentration C_0 = 7 ppm; Laser plus energy = 25.7–29.2 mJ.

and obtained results were compared with that of BiOCl, whose bandgap is close to P25. It was noticed that P25 owns higher total surface area (1 mmol, ~4.0 m^2) in the reaction than that of as-prepared BiOCl catalyst (1 mmol, ~0.45 m^2), and actual particle size of P25 is far lower than that of as-prepared BiOCl catalyst and such smaller size may contribute to higher quantum yield [30]. Our results revealed that the photocatalytic response of both the catalysts were similar for the decolorization of Rh 6G (Fig. 8a), and the highest PE values for BiOCl and P25 were estimated at 6.5% and 8.3% (at 15 min, as given in Fig. 8b), respectively. These results demonstrated that the specific surface area and bandgap of the photocatalysts may not be the most dominated reasons for photocatalytic decolorization of dye molecules from aqueous solutions. Therefore, it is necessary to discuss the mechanism deeply in terms of their band structure. Previously, ultraviolet photoelectron spectroscopy (UPS) [31], flatband-potential-determination based photoeletrochemical techniques [32–34] were two important methods to test the electrochemical potentials of conduction band (CB) and valence band (VB). Recently, a theoretical method based on the absolute (or Mullikan) electronegativity was used widely to predict band position of semiconductors and such simple method can be in good agreement with the experimental results for semiconductor compounds [35–38].

In this study, the band edge potentials of CB/VB of BiOCl and TiO_2 semiconductors were theoretically speculated and compared (as displayed in Table 3), assuming the bandgap values of BiOCl and TiO_2 are 3.4 eV and 3.2 eV, respectively. The calculated results revealed that the VB top potential of BiOCl (~3.56 eV) was more positive than that of the TiO_2 (~2.91 eV) because of its higher absolute electronegativity. The lower position of the VB band edge for BiOCl could be a significant reason during the photocatalytic process, which implied a stronger oxidization ability of the photogenerated holes (displayed in Fig. 8c). Previously, Jiang et al. [39] studied and discussed the photocatalytic degradation mechanism of methyl orange on BiOBr semiconductor through band edge calculation as well, suggesting the availability of this theoretical method for bandedge calculations of such bismuth oxyhalides series semiconductor compounds. However, one recent research carried out by Chai et al. [8] suggested that the VB band edge of BiOCl is ~2.4 eV (SHE) which was calculated by density functional theory (DFT) method and is very different from our result. Although the obvious error of DFT method for the band-structure parameters calculation (such like bandgap value) has been widely known [40], the results difference is still unclear and further work needs to be done in the future. On the other hand, previous density functional theory (DFT) analysis also suggested that the lowest unoccupied orbitals

Table 3
Relevant parameters of Ti, O, Bi, Cl atoms (ionization energy, atomic electron affinity and absolute electronegativity) and TiO_2, BiOCl semiconductors (absolute electronegativity, bandgap and electrochemical potentials of CB/VB band edges).

Element	Elements			Catalysts	Semiconductors			
	Atomic[a] ionization energy	Atomic[a] electron affinity	Absolute electronegativity		Bandgap	Absolute electronegativity	CB band edge electrochemical potential	VB band edges electrochemical potential
Ti	6.82812	0.079	3.45356	TiO_2	3.2	5.81193	-0.28807	2.91193
Bi	7.2855	0.942362	4.11393					
Cl	12.96763	3.612724	8.29018	BiOCl	3.4	6.35901	0.15901	3.55901
O	13.61805	1.4611096	7.53958					

[a] The relevant data were selected from [44].

(LUMO) in BiOCl crystals, which was mainly composed of Bi_{6p}, O_{2p}, and Cl_{3p} states, were supposed to be much more dispersed and it could be deduced that such configuration may be more favorable for the charge carrier transportation (an excited electron to travel a longer distance) in BiOCl crystals [41], compared to the 3d orbitals dominated in TiO_2 LUMO [2].

As a heterogeneous photocatalyst, the chemical stability in water and irradiation is an important issue related to the practical use of the photocatalyst in the area of water purification. Thus in order to investigate the stability of as-prepared BiOCl photocatalyst, we examined the XRD pattern of BiOCl crystal after 50 min photocatalysis under incident laser energy of ~60 mJ. The result given in Fig. 9 indicates that the apparent changes of BiOCl crystal structure cannot be found and all the diffraction peaks are in agreement with those of the tetragonal BiOCl phase before laser irradiation, demonstrating the excellent chemical stability of as-prepared photocatalyst.

A possible initial process on photocatalytic decolorization of Rh 6G molecules from water phase over BiOCl catalyst can be achieved on the basis of the discussions above. As a typical kind of a cationic dye with $pK_a = 7.5$ [42], the ionic Rh 6G molecules adsorbed on the surface of BiOCl crystals through electrostatic or intermolecular force and this process mainly followed the pseudo-second-order kinetic process and the rate-controlling step of external diffusion. A recent work reported by Chen et al. [43] showed that the electrons from CB of BiOCl can directly reduce either chlorine radical or the azo-bond of methyl orange molecules (which was used as model pollutant) during the photocatalytic process, and hydroxyl radical (•OH) was considered as the main oxidative species in the BiOCl photocatalysis process. Therefore it is reasonable that the following process would take place during the UV-laser induced photocatalysis over BiOCl semiconductor:

$$BiOCl \xrightarrow{355\,nm\ laser\text{-}excitation} BiOCl(e_{CB}^{-} + h_{VB}^{+})$$
$$h_{VB}^{+} + Cl^{-}(surface) \rightarrow {}^{\bullet}Cl(bonded)$$
$${}^{\bullet}Cl(bonded) + e_{CB}^{-} \rightarrow Cl^{-}(ionized)$$
$$h_{VB}^{+} + OH^{-}(H_2O) \rightarrow {}^{\bullet}OH$$
$${}^{\bullet}OH + Rh.6G^{+} \rightarrow \text{decolorization/further mineralization}$$

Thus the adsorbed Rh 6G molecules were further decolorized or decomposed/oxidized by hydroxyl radicals which were formed from the valence band of BiOCl semiconductor.

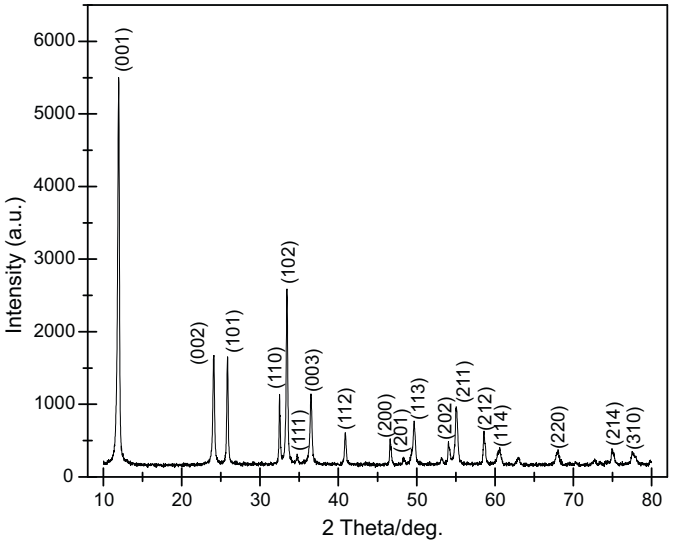

Fig. 9. XRD pattern of BiOCl recorded after 355 nm laser irradiation in Rh 6G aqueous solutions for 50 min.

4. Conclusions

The present study described the interfacial sorption and 355 nm-pulsed-laser induced photocatalytic decolorization behaviors of Rh 6G molecules in aqueous suspensions of as-prepared BiOCl. The sorption kinetics and isotherm of Rh 6G on BiOCl catalyst were investigated. The pseudo-second-order model can well describe the sorption kinetics of Rh 6G on BiOCl catalyst and the intraparticle diffusion model can relatively well fit its sorption in the initial stage. The sorption isotherm shows that the maximum sorption capacities of Rh 6G on BiOCl were 6.26626 mg/g according to the Langmuir model. The effect of catalyst dosage, initial concentration of Rh 6G and laser pulse energy on photocatalytic process was studied. Almost complete (~95%) decolorization of dye was achieved within 50 min of irradiation, and the highest PE value can be obtained at 13% after photocatalysis for 10 min as well. BiOCl exhibited similar photocatalytic activity to P25 under identical conditions possibly due to a stronger oxidization ability of the photo-generated holes in BiOCl semiconductor. The photocatalyst BiOCl was found to be chemically stable under the applied laser irradiation process.

Acknowledgements

This work was financially supported by Center of Excellence in Nanotechnolgy (CENT), and KFUPM through NSTIP program under Project #08-NAN93-4.

References

[1] M.R. Hoffmann, S.T. Martin, W. Choi, D.W. Bahnemann, Environmental applications of semiconductor photocatalysis, Chem. Rev. 95 (1995) 69–96.
[2] K. Zhang, C. Liu, F. Huang, C. Zheng, W. Wang, Study of the electronic structure and photocatalytic activity of the BiOCl photocatalyst, Appl. Catal. B: Environ. 68 (2006) 125–129.
[3] W. Wang, F. Huang, X. Lin, *x*BiOI–(1 – *x*)BiOCl as efficient visible-light-driven photocatalysts, Scripta Mater. 56 (2007) 669–672.
[4] W. Wang, F. Huang, X. Lin, J. Yang, Visible-light-responsive photocatalysts xBiOBr-(1 – *x*)BiOI, Catal. Commun. 9 (2008) 8–12.
[5] X. Zhang, Z. Ai, F. Jia, L. Zhang, Generalized one-pot synthesis, characterization, and photocatalytic activity of hierarchical BiOX (X = Cl, Br, I) nanoplate microspheres, J. Phys. Chem. C 112 (2008) 747–753.
[6] H. An, Y. Du, T. Wang, C. Wang, W. Hao, J. Zhang, Photocatalytic properties of BiOX (X = Cl, Br, and I), Rare Metals 27 (2008) 243–250.

[7] Z. Ai, W. Ho, S. Lee, L. Zhang, Efficient photocatalytic removal of NO in indoor air with hierarchical bismuth oxybromide nanoplate microspheres under visible light, Environ. Sci. Technol. 43 (2009) 4143–4150.
[8] S.Y. Chai, Y.J. Kim, M.H. Jung, A.K. Chakraborty, D. Jung, W.I. Lee, Heterojunctioned BiOCl/Bi_2O_3, a new visible light photocatalyst, J. Catal. 262 (2009) 144–149.
[9] X. Chang, J. Huang, Q. Tan, M. Wang, G. Ji, S. Deng, G. Yu, Photocatalytic degradation of PCP–Na over BiOI nanosheets under simulated sunlight irradiation, Catal. Commun. 10 (2009) 1957–1961.
[10] X. Chang, J. Huang, C. Cheng, Q. Sui, W. Sha, G. Ji, S. Deng, G. Yu, BiOX (X = Cl, Br, I) photocatalysts prepared using $NaBiO_3$ as the Bi source: characterization and catalytic performance, Catal. Commun. 11 (2010) 460–464.
[11] S. Wu, C. Wang, Y. Cui, T. Wang, B. Huang, X. Zhang, X. Qin, P. Brault, Synthesis and photocatalytic properties of BiOCl nanowire arrays, Mater. Lett. 64 (2010) 115–118.
[12] K. Zhao, X. Zhang, L. Zhang, The first BiOI-based solar cells, Electrochem. Commun. 11 (2009) 612–615.
[13] X. Chang, J. Huang, C. Cheng, W. Sha, X. Li, G. Ji, S. Deng, G. Yu, Photocatalytic decomposition of 4-*t*-octylphenol over $NaBiO_3$ driven by visible light: catalytic kinetics and corrosion products characterization, J. Hazard. Mater. 173 (2010) 765–772.
[14] A. Hameed, M.A. Gondal, Z.H. Yamani, Effect of transition metal doping on photocatalytic activity of WO_3 for water splitting under laser illumination: role of 3d-orbitals, Catal. Commun. 5 (2004) 715–719.
[15] M.A. Gondal, A. Hameed, Z.H. Yamani, A. Suwaiyan, Production of hydrogen and oxygen by water splitting using laser induced photo-catalysis over Fe_2O_3, Appl. Catal. A: Gen. 268 (2004) 159–167.
[16] M. Qamar, M.A. Gondal, K. Hayat, Z.H. Yamani, K. Al-Hooshani, Laser-induced removal of a dye C.I. Acid Red 87 using n-type WO_3 semiconductor catalyst, J. Hazard. Mater. 170 (2009) 584–589.
[17] M.A. Gondal, M.N. Sayeed, Z. Seddigi, Laser enhanced photo-catalytic removal of phenol from water using p-type NiO semiconductor catalyst, J. Hazard. Mater. 155 (2008) 83–89.
[18] M.A. Gondal, M.A. Dastageer, A. Khalil, Synthesis of nano-WO_3 and its catalytic activity for enhanced antimicrobial process for water purification using laser induced photo-catalysis, Catal. Commun. 11 (2009) 214–219.
[19] L. Guo, G. Ji, X. Chang, M. Zheng, Y. Shi, Y. Zheng, Microwave-assisted synthesis of Sb_2Se_3 submicron tetragonal tubular and spherical crystals, Nanotechnology 21 (2010) 035606.
[20] X. Chang, G. Ji, K. Shen, L. Pan, Y. Shi, Y. Zheng, Fabrication of nanowire-like cuprous oxide in aqueous solutions of a triblock copolymer, J. Alloy Compd. 482 (2009) 240–245.
[21] Y.S. Ho, G. McKay, Pseudo-second order model for sorption processes, Process Biochem. 34 (1999) 451–465.
[22] Q. Yu, R. Zhang, S. Deng, J. Huang, G. Yu, Sorption of perfluorooctane sulfonate and perfluorooctanoate on activated carbons and resin: kinetic and isotherm study, Water Res. 43 (2009) 1150–1158.
[23] X. Yang, B. Al-Duri, Kinetic modeling of liquid-phase adsorption of reactive dyes on activated carbon, J. Colloid Interface Sci. 287 (2005) 25–34.
[24] I. Langmuir, The constitution and fundamental properties of solids and liquids. Part i. Solids, J. Am. Chem. Soc. 38 (1916) 2221–2295.
[25] H.M.F. Freundlich, Über die adsorption in lösungen, Z. Phys. Chem. 57 (1906) 385–470.
[26] X. Chang, G. Yu, J. Huang, Z. Li, S. Zhu, Pi. Yu, C. Cheng, S. Deng, G. Ji, Enhancement of photocatalytic activity over $NaBiO_3$/BiOCl composite prepared by an in situ formation strategy, Catal. Today 153 (2010) 193–199.
[27] X. Chang, G. Ji, Q. Sui, J. Huang, G. Yu, Rapid photocatalytic degradation of PCP–Na over $NaBiO_3$ driven by visible light irradiation, J. Hazard. Mater. 166 (2009) 728–733.
[28] D.W. Chen, A.K. Ray, Photodegradation kinetics of 4-nitrophenol in TiO_2 suspension, Water Res. 32 (1998) 3223–3234.
[29] E. Kusvuran, A. Samil, O.M. Atanur, O. Erbatur, Photocatalytic degradation kinetics of di- and tri-substituted phenolic compounds in aqueous solution by TiO_2/UV, Appl. Catal. B: Environ. 58 (2005) 211–216.
[30] H. Gerischer, Photocatalysis in aqueous solution with small TiO_2 particles and the dependence of the quantum yield on particle size and light intensity, Electrochim. Acta 40 (1995) 1277–1281.
[31] B. Xu, W.F. Zhang, X.-Y. Liu, J.H. Ye, W.H. Zhang, L. Shi, X.G. Wan, J. Yin, Z.G. Liu, Photophysical properties and electronic structures of the perovskite photocatalysts $Ba_3NiM_2O_9$ (M = Nb, Ta), Phys. Rev. B 76 (2007) 125109.
[32] Y. Matsumoto, M. Omae, I. Watanabe, E. Sato, Photoelectrochemical properties of the Zn–Ti–Fe spinel oxides, J. Electrochem. Soc. 133 (1986) 711–716.
[33] Y. Matsumoto, Energy positions of oxide semiconductors and photocatalysis with iron complex oxides, J. Solid State Chem. 126 (1996) 227–234.
[34] R. Brahimi, Y. Bessekhouad, A. Bouguelia, M. Trari, $CuAlO_2$/TiO_2 heterojunction applied to visible light H_2 produ, J. Photochem. Photobiol. A 186 (2007) 242–247.
[35] W. Yao, J. Ye, A new efficient visible-light-driven photocatalyst $Na_{0.5}Bi_{1.5}VMoO_8$ for oxygen evolution, Chem. Phys. Lett. 450 (2008) 370–374.
[36] J. Tang, Z. Zou, J. Ye, Efficient photocatalysis on $BaBiO_3$ driven by visible light, J. Phys. Chem. C 111 (2007) 12779–12785.
[37] M. Long, W. Cai, J. Cai, B. Zhou, X. Chai, Y. Wu, Efficient photocatalytic degradation of phenol over Co_3O_4/$BiVO_4$ composite under visible light irradiation, J. Phys. Chem. B 110 (2006) 20211–20216.
[38] X. Lin, J. Xing, W. Wang, Z. Shan, F. Xu, F. Huang, Photocatalytic activities of heterojunction semiconductors Bi_2O_3/$BaTiO_3$: a strategy for the design of efficient combined photocatalysts, J. Phys. Chem. C 111 (2007) 18288–18293.
[39] Z. Jiang, F. Yang, G. Yang, L. Kong, M.O. Jones, T. Xiao, P.P. Edwards, The hydrothermal synthesis of BiOBr flakes for visible-light-responsive photocatalytic degradation of methyl orange, J. Photochem. Photobiol. A: Chem. 212 (2010) 8–13.
[40] W. Huang, Q. Zhu, Electronic structures of relaxed BiO*X* (*X* = F, Cl, Br, I) photocatalysts, Comput. Mater. Sci. 43 (2008) 1101–1108.
[41] D. Wang, T. Kako, J. Ye, Efficient photocatalytic decomposition of acetaldehyde over a solid-solution perovskite $(Ag_{0.75}Sr_{0.25})(Nb_{0.75}Ti_{0.25})O_3$ under visible-light irradiation, J. Am. Chem. Soc. 130 (2008) 2724–2725.
[42] K. Tarun, Khurana, G. Juan, Santiago, Effects of carbon dioxide on peak mode isotachophoresis: simultaneous preconcentration and separation, Lab Chip 9 (2009) 1377–1384.
[43] F. Chen, H. Liu, S. Bagwasi, X. Shen, J. Zhang, Photocatalytic study of BiOCl for degradation of organic pollutants under UV irradiation, J. Photochem. Photobiol. A: Chem. 215 (2010) 76–80.
[44] D.R. Lide, Handbook of Chemistry and Physics, 87th ed., CRC Press, 2006–2007.